Antireflective Nanostructures for CPV

Jeronimo Buencuerpo, Lorena Torne, Raquel Alvaro, Jose Manuel Llorens, María Luisa Dotor, and Jose Maria Ripalda[1, a)]

[1] *IMM-Instituto de Microelectronica de Madrid (CNM-CSIC), E-28760 Tres Cantos, Madrid, Spain*
[a)] Corresponding author: j.ripalda@csic.es

Abstract. We have optimized a periodic antireflective nanostructure. The optimal design has a theoretical broadband reflectivity of 0.54% on top of GaInP with an AlInP window layer. Preliminary fabrication attempts have been carried out on top of GaAs substrates. Due to the lack of a window layer, and the need to fine tune the fabrication process, the fabricated nanostructures have a reflectivity of 3.1%, but this is already significantly lower than the theoretical broadband reflectance of standard MgF_2/ZnS bilayers (4.5%).

INTRODUCTION

Nano-structuring the surfaces of solar cells presents the opportunity to engineer the optical response with more degrees of freedom than using only flat layers. Particularly, it allows to exploit diffraction effects not present in conventional antireflective coatings (ARCs) based on destructive interference [1] and gradual index matching [2]. Diffraction does not occur if the grating period is smaller than the light wavelength. But the wavelength is much shorter inside the solar cell than in air or glass, thus by placing the grating at an interface with a high refractive index contrast, and choosing the grating period to be slightly smaller than the shortest wavelength of interest, all the light diffracted by the grating (by addition of a reciprocal lattice wave-vector) propagates forward into the solar cell, reducing reflection [3,4]. The intensity of the effect depends on the scattering efficiency of the grating, which in turn depends on the refractive index contrast, among other factors. A viable approach to overcome the difficulty of finding materials with the appropriate refractive indexes is based on porous or mixed layers, but the maximum usable refractive index is still limited by the choice of materials with low absorption in the wavelength range of interest.

Perl et al. recently presented a high performance (2.8% broad-band reflection) hybrid ARC design for CPV applications that used sub-wavelength glass nano-structures as a graded index layer and an interferential multilayer [5]. Because of the small refractive index contrast between air and glass, diffraction effects were negligible in this design. Diffraction based antireflective nano-structures have been demonstrated by nano-structuring a semiconductor material, thus attaining a high refractive index contrast [6-10], but this approach is not advantageous for III-V solar cells due to unacceptably high surface recombination losses. A few examples of anti-reflective nano-structures specially adapted for III-V solar cells can be found in the literature, but most results are still far from optimal due to the complexity of the problem [11-14]. The herein proposed periodic nanostructured ARCs are based on a periodic array of silicon nitride nano-cones on a thin titanium oxide layer for index matching with the substrate. The diffraction efficiency can be further increased by fabricating the nano-cones on higher refractive index materials such as tantalum oxide or titanium oxide, but at the expense of higher parasitic absorption losses.

The fabricated periodic nanostructures work as an effective medium with a graded index for wavelengths larger than the lattice parameter, and as diffraction grating for wavelengths shorter than the lattice parameter. Because the incident light is diffracted off-axis, the average optical path length is increased, allowing for complete light absorption using thinner semiconductor layers. This is advantageous when the charge carrier diffusion lengths or other constraints, such as epitaxial strain due to lattice mismatch, limit the absorber thickness. Although in the present work we have optimized our structures for maximum transmission into the substrate, the structures can also

be optimized for maximum absorption with a thin absorber [15], or for maximum efficiency using a detailed balance model [16].

Other optical losses, such as those caused by the top contacts, can also be minimized by engineering at the nano-scale. In a previous work we have theoretically and experimentally shown that silver top contact wires 400 - 600 nm wide have an effective shadow that is only a fraction of their projected area [17].

THEORETICAL OPTIMIZATION

The proposed structure is a square lattice of silicon nitride cones on top of a thin silicon nitride layer. An additional titanium oxide layer is included for refractive index matching between the silicon nitride and the AlInP window layer (Fig 1a). The substrate is GaInP. We have also studied the case where the whole ARC is fabricated on titanium oxide, at the expense of increased parasitic absorption. The transmission has been calculated using rigorous coupled wave analysis (RCWA) for a broadband spectrum ranging from 0.69 to 3.5 eV [18].

A critical aspect of these calculations is the choice of refractive index for titanium oxide. The titanium oxide phase with the highest refractive index and its lowest absorption is only attainable using very high temperature synthesis methods that are incompatible with solar cell processing. As a consequence, theoretical estimates of optical losses in ARCs based on titanium oxide are often over optimistic [5]. We have chosen instead to use the experimentally measured refractive index of titanium oxide thin films synthesized at low temperatures [19]. The optical properties of all other materials are taken from standard sources [18].

All of the structure dimensions are optimized for maximum transmission, and the resulting parameters are presented in Table I. The AlInP window layer has a fixed thickness of 15 nm. The obtained transmittance is robust against fabrication errors with a 10% error in any dimension having only a small effect on transmittance (< 0.05%). The resulting theoretical transmission spectra are shown in Fig. 1b.

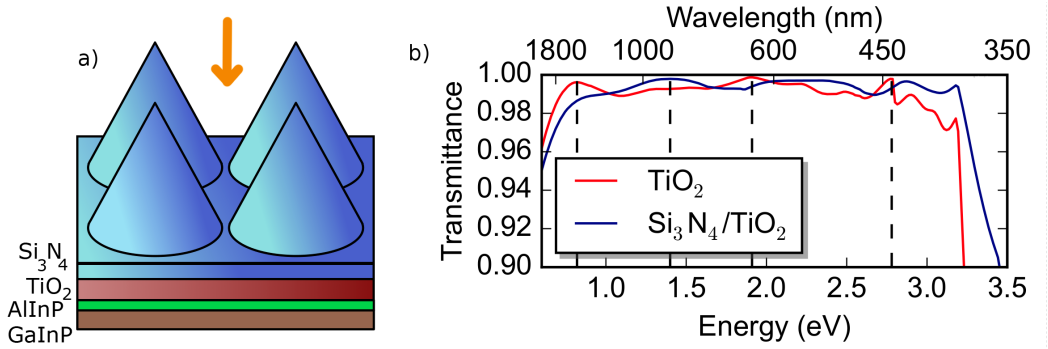

FIGURE 1. a) Model of the nano-cones based diffraction grating. The nano-cones are made of a low absorption material (such as silicon nitride) on top of an index titanium oxide thin film. The AInP window layer is also depicted on top of the GaInP substrate. b) Transmission spectra of the proposed structure after optimization of all dimensional parameters for maximum broadband transmission.

TABLE 1. Dimensions of the optimized nano-cones. The thicknesses of the silicon nitride and titanium oxide thin films are d_{ni} and d_{ox}, respectively.

	***Period* (nm)**	***Radius* (nm)**	***Height* (nm)**	d_{ni}**(nm)**	d_{ox}**(nm)**
TiO_2	444	222	534	-	43
Si_3N_4 / TiO_2	344	163	512	49	51

An additional benefit of the nanostructured ARC is a slightly higher angular acceptance compared to a standard Mg_2F/ZnS bilayer optimized for the same spectral range, as shown in Fig. 2.

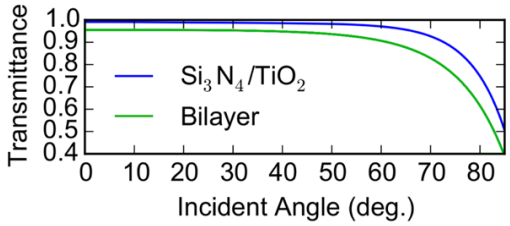

FIGURE 2. Transmission as a function of incidence angle for the optimized silicon nitride nano-cones and a similarly optimized MgF_2/ZnS bilayer.

The used methodology allows to obtain the photon flux in each diffraction order, and thus the diffraction efficiency. From these efficiencies and the diffraction angle corresponding to each diffraction order we have obtained the averaged enhancement of the optical path length due to scattering by the diffraction grating (Fig. 3).

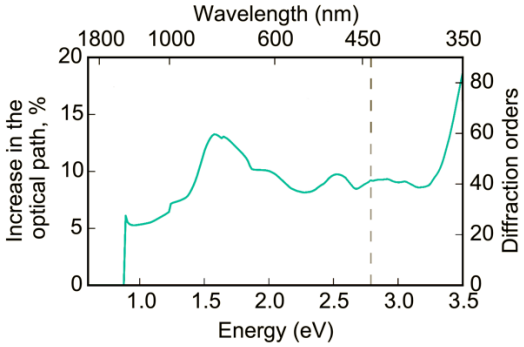

FIGURE 3. Optical path length enhancement for the titanium oxide cones. As seen in Table 2, the enhancement is larger for the nano-cones with the higher refractive index.

Table 2 summarizes the optical losses and the optical path length enhancement for the silicon nitride and titanium oxide based cones. The unavoidable trade-off between scattering efficiency and parasitic absorption is apparent in these results. The low reflectance is largely due to the inhibition of reflected diffraction.

TABLE 2. Optical losses and optical path enhancement for the silicon nitride nano-cones and the titanium oxide nano-cones.

	Reflectivity	**Abs. losses**	**Transmission**	**Opt. path**
TiO_2	0.74 %	1.04 %	98.22 %	5 – 15 %
Si_3N_4 / TiO_2	0.54 %	0.34 %	99.12 %	1 – 7 %

By comparing the simulations of our TiO_2 nanocone gratings with simulations based on an equivalent effective graded index, we show in Fig. 4 that the obtained high transmission cannot be accounted for disregarding the effects of diffraction. For simplicity, we have neglected chromatic dispersion in this comparison. Further details are given in ref. 18.

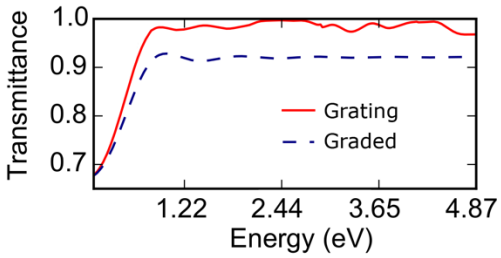

FIGURE 4. Transmission for our nano-cone based grating structure, and an equivalent graded index medium with the same average refractive index as a function of depth inside the structure. The larger transmission for the grating is due to diffraction effects absent in the graded index medium.

FABRICATION

Preliminary fabrication efforts to test the proposed ARCs have been done on GaAs substrates using laser interference patterning (LIL) of a photoresist that is subsequently used as a dry etching mask for patterning the silicon nitride layer [20]. The initial step for the fabrication was the deposition of 51 nm of titanium oxide using atomic layer deposition. Subsequently 616 nm of silicon nitride were deposited using plasma enhanced chemical vapour deposition. Both layers were deposited at a relatively low temperature (200 ºC) to ensure process compatibility with a wide range of CPV technologies. The samples were covered with 150 nm of diluted S1805 photoresist. The sample was then exposed twice in two orthogonal directions using LIL with a Lloyd mirror configuration and a 405 nm spatially filtered laser beam [21].

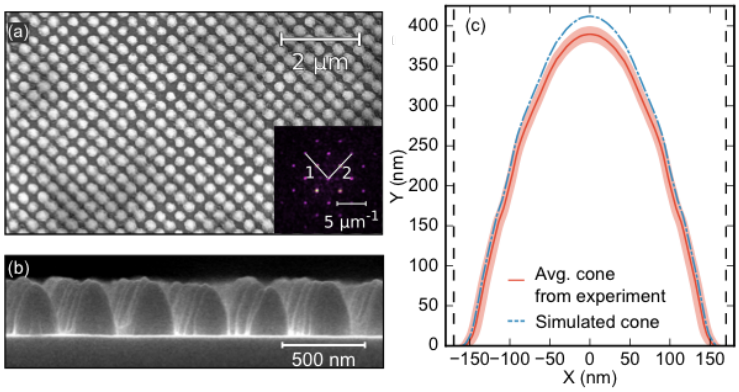

FIGURE 5. a) SEM image of the nanostructure, inset Fast Fourier transform of the structure. (b) Cross sectional SEM image used to estimate the mean profile. (c) Mean profile of the cones, scaled to the experimental data (red line), and optimal profile extracted from the reflectance fitting (blue dash-dotted line). The vertical dashed lines are the limits of the unit cell.

The pattern was transferred to the silicon nitride layer using RIE with a N_2 and CHF_3 plasma. Fig.5(a,b) shows the sample after the etching process. Comparison of the average profile extracted from the SEM images (Fig. 5c) with the optimal parameters in Table 1 reveals that, except for the reduced height and slightly rounded off tips, we have met our fabrication target.

EXPERIMENTAL RESULTS

To be able to detect spatial variations of the reflectance on the sample surface, the reflectance was measured using a 20X magnification objective lens (NA = 0.4) at the lower vertical arm of a beamsplitter. The signal reflected from the sample was collected by the objective and sent through the beam splitter to a lens focused on a silicon photodiode on the upper arm of the beam splitter. Monochromatic illumination entered from the side into the beamsplitter. The set up was calibrated by measuring samples with known reflectance. This also served to partially compensate for the limited light collection angle. The bounds of our experimental spectra (440 nm to 870 nm) are limited by the position of the GaAs absorption edge, the spectral distribution of our illumination source, and the transmission of the optical components in the set up. The reflectivity measurements were compared with the simulations results obtained using the scattering matrix method on an average unit cell representative of the distribution of the real nanostructures. An initial set of dimensions describing the size and shape of the nanostructures was obtained from electron microscopy images and profilometer measurements and then slightly (<5% change) refined by fitting the simulations to the experimental reflectivity.

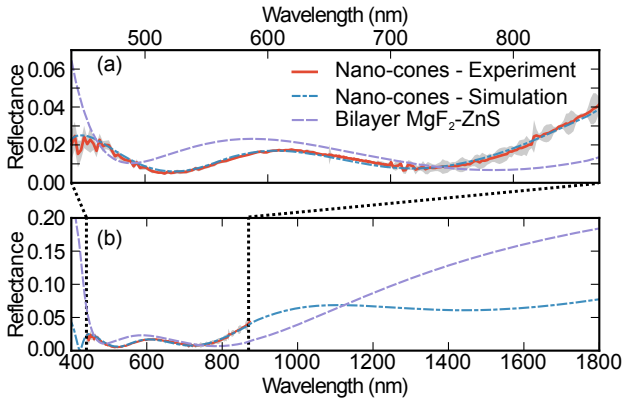

FIGURE 6. (a) Experimental reflectance (red), experimental standard deviation (light gray), theoretical reflectance (dashed-dotted blue) and theoretical reflectance of an optimal bilayer (MgF_2ZnS) (dashed purple). (b) Theoretical reflectance in an extended spectral range.

The experimental and simulated reflectance data are shown in Fig 6(a). Fig. 6(b) shows the reflectance resulting from our fitting in an extended spectral range from 400 to 1800 nm in comparison with the optimized bilayer. In the visible and near infrared range of the spectrum (440 nm - 870 nm), the nanostructures lead to a 1.4% spectrally averaged reflectance. Using the model data to extend the integration range to 400 nm - 1800 nm, the obtained spectrally averaged reflectance is 3.1%.

CONCLUSIONS

The fabricated nanostructured antireflective coating on a GaAs substrate without window layer has a broadband reflectance of 3.1%, surpassing what can theoretically be achieved with a standard bilayer MgF_2/ZnS ARC. Our simulations predict that including an AlInP window layer, a GaInP top cell, and fine tuning the fabrication process to obtain slightly taller and sharper nano-cones, should result in broadband reflection losses of 0.54% and absorption losses of 0.34% (broadband transmission > 99%).

ACKNOWLEDGMENTS

We acknowledge financial support by MINECO (TEC2015-64189-C3-2-R) and CAM (S2013/MAE-2780).

REFERENCES

1. M. Victoria, C. Domínguez, I. Antón & G. Sala. Antireflective coatings for multijunction solar cells under wide-angle ray bundles. Optics Express 20, 8136–8147 (2012).
2. W. H. Southwell. Gradient-index antireflection coatings. Optics Letters 8, 584–586 (1983).
3. E. B. Grann, M. G. Moharam & D. A. Pommet. Optimal design for antireflective tapered two-dimensional subwavelength grating structures. Journal of the Optical Society of America A 12, 333–339 (1995).
4. Z. Yu, A. Raman & S. Fan. Fundamental limit of nanophotonic light trapping in solar cells. Proceedings of the National Academy of Sciences 107, 17491–17496 (2010).
5. E. E. Perl, C.-T. Lin, W. E. McMahon, D. J. Friedman & J. E. Bowers. Ultrabroadband and Wide-Angle Hybrid Antireflection Coatings With Nanostructures. IEEE Journal of Photovoltaics 4, 962–967 (2014).
6. S. A. Boden & D. M. Bagnall. Optimization of moth-eye antireflection schemes for silicon solar cells. Progress in Photovoltaics: Research and Applications 18, 195–203 (2010).
7. J. Tommila, A. Aho, A. Tukiainen, V. Polojärvi, J. Salmi, T. Niemi & M. Guina. Moth-eye antireflection coating fabricated by nanoimprint lithography on 1 eV dilute nitride solar cell. Progress in Photovoltaics: Research and Applications 21, 1158–1162 (2013).
8. K. X. Wang, Z. Yu, V. Liu, Y. Cui & S. Fan. Absorption Enhancement in Ultrathin Crystalline Silicon Solar Cells with Antireflection and Light-Trapping Nanocone Gratings. Nano Letters 12, 1616–1619 (2012).
9. I. Prieto, B. Galiana, P. A. Postigo, C. Algora, L. J. Martínez & I. Rey-Stolle. Enhanced quantum efficiency of Ge solar cells by a two-dimensional photonic crystal nanostructured surface. Applied Physics Letters 94, 191102 (2009).
10. M. Otto, M. Algasinger, H. Branz, B. Gesemann, T. Gimpel, K. Füchsel, T. Käsebier, S. Kontermann, S. Koynov, X. Li, V. Naumann, J. Oh, A. N. Sprafke, J. Ziegler, M. Zilk & R. B. Wehrspohn. Black Silicon Photovoltaics. Advanced Optical Materials 3, 147–164 (2015).
11. J. W. Leem, J. Su Yu, D.-H. Jun, J. Heo & W.-K. Park. Efficiency improvement of III–V GaAs solar cells using biomimetic TiO2 subwavelength structures with wide-angle and broadband antireflection properties. Solar Energy Materials and Solar Cells 127, 43–49 (2014).
12. M.-M. Hung, H.-V. Han, C.-Y. Hong, K.-H. Hong, T.-T. Yang, P. Yu, Y.-R. Wu, H.-Y. Yeh & H.-C. Huang. Compound biomimetic structures for efficiency enhancement of Ga0.5In0.5P/GaAs/Ge triple-junction solar cells. Optics Express 22, A295–A300 (2014).
13. C.-H. Sun, B. J. Ho, B. Jiang & P. Jiang. Biomimetic subwavelength antireflective gratings on GaAs. Optics Letters 33, 2224–2226 (2008).
14. S. L. Diedenhofen, G. Grzela, E. Haverkamp, G. Bauhuis, J. Schermer & J. G. Rivas. Broadband and omnidirectional anti-reflection layer for III/V multi-junction solar cells. Solar Energy Materials and Solar Cells 101, 308–314 (2012).
15. J. Buencuerpo, J. M. Llorens, P. Zilio, W. Raja, J. Cunha, A. Alabastri, R. P. Zaccaria, A. Martí & T. Versloot. Light-trapping in photon enhanced thermionic emitters. Optics Express 23, A1220 (2015).
16. J. Buencuerpo, J. M. Llorens, M. L. Dotor & J. M. Ripalda. Photon management with nanostructures on concentrator solar cells. Applied Physics Letters 103, 083901–083901 (2013).
17. E. San Román, A. Vitrey, J. Buencuerpo, I. Prieto, J. M. Llorens, A. García- Martín, B. Alén, A. Chaudhuri, A. Neumann, S. R. J. Brueck & et al. Cloaking of solar cell contacts at the onset of Rayleigh scattering. Scientific Reports 6, 28669 (2016).
18. J. Buencuerpo, J. M. Llorens, M. L. Dotor & J. M. Ripalda. Broadband antireflective nano-cones for tandem solar cells. Optics Express 23, A322 (2015).
19. S. Tanemura, L. Miao, P. Jin, K. Kaneko, A. Terai & N. Nabatova-Gabain. Optical properties of polycrystalline and epitaxial anatase and rutile TiO2 thin films by rf magnetron sputtering. Applied Surface Science 212–213, 654–660 (2003).
20. J. Buencuerpo, L. Torne, R. Alvaro, J. M. Llorens, M. L. Dotor, and J. M. Ripalda, "Nano-cones for broadband light coupling to high index substrates", Scientific Reports, 6, 3868 (2016).
21. C. P. Fucetola, H. Korre & K. K. Berggren. Low-cost interference lithography. Journal of Vacuum Science & Technology B: Microelectronics and Nanometer Structures 27, 2958 (2009).